Lentinan stabilized bimetallic $PdPt_3$ dendritic nanoparticles with enhanced oxidase-like property for L-cysteine detection

Ziyi Ma[a], Le Dong[b], Bingjie Zhang[b], Bo Liang[a], Liqiu Wang[b], Guanglong Ma[c], Longgang Wang[a,b]**

a. State Key Laboratory of Metastable Materials Science and Technology, College of Materials Science and Engineering, Yanshan University, Qinhuangdao, 066004, China

b. Key Laboratory of Applied Chemistry, Nano-biotechnology Key Lab of Hebei Province, College of Environmental and Chemical Engineering, Yanshan University, Qinhuangdao, 066004, China

c. Centre for Cancer Immunology, Faculty of Medicine, University of Southampton, Southampton, SO166YD, UK

* *Corresponding author* liangbo@ysu.edu.cn; lgwang@ysu.edu.cn

Abstract

The development of nanozymes with enhanced catalytic activity has been drawing great interest. Lentinan with special structure may be used to prepare bimetallic nanomaterials to enhance their catalytic activity. Herein, lentinan stabilized $PdPt_3$ dendritic nanoparticles ($PdPt_3$-LNT NDs) were prepared through reduction of Na_2PdCl_4 and K_2PtCl_4 with a molar ratio of 1:3 using lentinan as a biological template. $PdPt_3$-LNT NDs had dendritic shape with size of 10.76±1.82 nm. $PdPt_3$-LNT NDs had the hydrodynamic size about 25.7 nm and the zeta potential between -1.4 mV and -4.9 mV at different pH. Furthermore, $PdPt_3$-LNT NDs catalyzed 3,3',5,5'-tetramethylbenzidine (TMB) to produce oxidized TMB, suggesting their oxidase-like property. The catalytic activity of $PdPt_3$-LNT NDs was the highest when pH was 4 and the temperature was 40 °C. The catalytic mechanism was the generation of $\cdot O_2^-$ and $^1O_2$ from O_2 catalyzed by $PdPt_3$-LNT NDs. More importantly, L-cysteine detection method was set up based on the oxidase-like property of $PdPt_3$-LNT NDs. This method had wide linear range for 0-200 μM and low detection limit for 3.099 μM. Taken together, $PdPt_3$-LNT NDs have good potential applications in bio-related detection in the future.

Keywords: nanozyme, lentinan, colorimetric detection

1. Introduction

L-cysteine is one kind of the semi-essential amino acids, widely participates in activities in living organisms. L-cysteine is characterized by the presence of a

sulfhydryl group in its structure, which allows it to participate in the reduction process of cells and protect cells from toxic substances[1,2]. Normal physiological activities in living organisms are inseparable from a stable environment, which requires a stable concentration of L-cysteine in the environment. Dysregulation of L-cysteine metabolism can cause serious consequences [3]. Therefore, various methods for L-cysteine detection have been developed [4]. Colorimetric method is one of the popular methods to measure the L-cysteine concentration. The colorimetric detection performance of L-cysteine relies on the catalytic ability of enzyme. Therefore, it is important to improve the catalytic ability of enzyme.

The L-cysteine concentration can be detected using natural enzymes. However, natural enzymes have some drawbacks such as complicated extraction process, easy denaturation, and high cost[5]. Some nanoparticles exhibit enzyme-like catalytic activity under appropriate conditions, which are called nanozymes[6,7]. Nanozymes have many advantages such as easy storage, simple preparation, and easy control over natural enzymes[8]. There are many kinds of nanoparticles that can be used as nanozymes, including metal oxides[9,10], carbon-based nanomaterials[11], noble metal nanomaterials[10-13] and other nanomaterials[14,15]. Cerium oxide nanomaterials have good oxidase-like activity [16,17]. Noble metal nanoparticles stand out due to their high catalytic activity, mild synthesis conditions, and large specific surface area. Many noble metal nanoparticles have been used in the field of detecting L-cysteine [18]. Compared with Pt nanoparticles and Pd nanoparticles, the Pt-Pd bimetallic nanoparticles with synergistic effects have high catalytic activity such as PdPt composition nanowires[19] and Pt-Pd alloy networks[20,21]. The catalytic ability of bimetallic metal nanoparticles could be enhanced by tuning their composition[22]. The morphology of nanoparticles also affects the catalytic activity of nanozymes[23]. The special morphology of the nanozyme with increasing specific surface area enhances the catalytic activity[24]. Last, the high stability of nanozymes in solution contributes to high activity of nanozymes, which was due to high accessibility between catalytic center and substrates. Therefore, the composition, morphology and stability of

bimetallic nanomaterials are closely corelated with their catalytic activity [25-27].

Lentinus edodes is an edible fungus and widely eaten in daily life[28]. Lentinus edodes contains a variety of substances that may have medicinal value[29-31]. Lentinan (LNT) is the polysaccharide of lentinus edodes. LNT has the effects of lowering blood sugar, relieving cough and resolving phlegm. LNT is high molecular weight (300,000-800,000) biomacromolecules with water solubility. There are many hydroxyl groups and other functional groups in the structure of LNT[32]. These important groups can interact with metal precursors and reduce them to metal nanoparticles based on reductive properties of LNT. After the metal precursors are reduced, LNT is attached and covered to the metal nanoparticles. The steric hindrance effect of LNT prevents aggregation of metal nanoparticles in solution[33].

Antioxidant and soluble LNT has special β-glucan structure, LNT may be used to biomineralize bimetallic nanomaterials to enhance the catalytic activity of nanozymes. Herein, the hot water method was used to extract LNT [34,35]. LNT stabilized $PdPt_3$ dendritic nanoparticles ($PdPt_3$-LNT NDs) were prepared by a simple method. Extracted LNT was used as a stabilizer and reducing agent to produce metal seeds, and ascorbic acid acted as a reducing agent in the preparation method. $PdPt_3$-LNT NDs had dendritic morphologies with size 10.76±1.82 nm. 3,3',5,5'-tetramethylbenzidine (TMB) solution was oxidized to blue oxidized TMB (oxTMB) by $PdPt_3$-LNT NDs, indicating their oxidase-like property. The sulfhydryl group in L-cysteine inhibited the oxidization of TMB. The absorbance of oxTMB was detected by UV-Vis spectrophotometer. Therefore, the oxTMB absorbance depended on the L-cysteine concentration, and the concentration of L-cysteine can be measured by the catalytic oxidation of TMB by using $PdPt_3$-LNT NDs due to their oxidase-like property. The green synthetic $PdPt_3$-LNT NDs have great potential application in L-cysteine detection.

2. Experimental section

2.1 Materials and instruments

Lentinus edodes was obtained from local supermarket. Potasium tetrachloroplatinate (II) (K_2PtCl_4), sodium tetrachloropalladate (II) (Na_2PdCl_4),

hydrogen peroxide (H_2O_2), 3,3',5,5'-tetramethylbenzidine (TMB), terephthalic acid (TA), L-cysteine, ascorbic acid, acetic acid (Hac) and sodium acetate (NaAc) were purchased from Aladdin Reagent Co., Ltd. 1-butanol was purchased from Tianjin Chemical Reagent Supply and Marketing Company. Trichloromethane was purchased from Tianjin Jindong Tianzheng Fine Chemical Reagent Factory. 1,4-benzoquinone (BQ) was purchased from Shanghai Baishun Biotechnology Co., Ltd.

Transmission electron microscopy (TEM) was performed on a HT 7700. X-Ray diffractometer (XRD) equipment was D-max-2500/PC. Fourier transform infrared (FTIR) patterns were recorded using a E55-FRA106. X-ray photoelectron spectroscopy (XPS) was performed on a Thermo Scientific K-Alpha. The UV-Vis spectra were used a UV-TU1810 spectrophotometer. Fluorescence spectra were recorded using an F-7000. The laser particle size analyzer was carried on a Zetasizer Nano-ZS90. The molecular weight of LNT was determined by gel permeation chromatography-20A (GPC-20A). The concentration of metal elements was measured by inductively coupled plasma mass spectrometry (ICP-MS) XSeries II.

2.2 Preparation of $PdPt_3$-LNT NDs

LNT was extracted by using hot water extraction method [6]. Lentinus edodes was dried in a constant temperature oven at 50 °C after washing. Then Lentinus edodes was smashed into Lentinus edodes powder. Lentinus edodes powder was put into flask, dissolved in deionized water. After mixing and shaking, the mixture was kept in water at 90 ℃ for 3 h. The supernatant was collected and filtrated. H_2O_2 (30%) was added into the mixture, and the mixed solution was kept at 50 ℃ for 2 h. Savage reagent ($V_{chloromethane}$:$V_{n\text{-}butanol}$=5:1) was added into the mixture to remove the proteins. The crude polysaccharide solution was put into dialysis bag. Finally, the solution was placed in the freeze drier to get LNT powder. The purity of LNT was about 90%.

$PdPt_3$-LNT NDs were prepared with following procedure. 1 mL LNT (1 mg/mL) solution and 0.125 mL Na_2PdCl_4 (1 mM) were incubated at 50 ℃ for 6 h. After the solution cooled to room temperature, 0.375 mL K_2PtCl_4 (1 mM) was added into the solution. 100 μL ascorbic acid solution (0.1 M) was slowly added into the solution,

which was incubated at 60 ℃ for 12 h. The solution was dialyzed for 24 h to collect $PdPt_3$-LNT NDs solution. $PdPt_3$-LNT NDs solution was stored in a refrigerator at 4 °C for later use. In order to study the role of LNT, $PdPt_3$ nanoparticles ($PdPt_3$ NPs) were prepared without using LNT, where ascorbic acid was used as reducing agent. Other samples including Pd-LNT NPs, Pt-LNT NPs, PdPt NPs, Pd_3Pt NPs with the molar ratio of Na_2PdCl_4 to K_2PtCl_4 for 1:0, 0:1, 1:1, 3:1 had similar process, respectively.

2.3 Determination of the oxidase-like activity

100 μL samples (C_{pd}=0.078 mM) and 500 μL Hac-NaAc (pH=4, 0.2 M) were mixed and incubated in the constant temperature mixer at 25°C for 3 min; then 800 μL TMB (0.6 mM) was transferred, and the reaction was performed for 10 min at 25°C. Finally, the absorbance from 500 to 750 nm was measured by UV-Vis spectrometer.

2.4 Effects of pH and temperature on the oxidase-like activity

The effect of temperature on the activity of $PdPt_3$-LNT NDs was measured as follows. 100 μL $PdPt_3$-LNT NDs (C_{pd}=0.078 mM) solution and 500 μL Hac-NaAc (pH=4, 0.2 M) buffer solution were mixed and incubated at different temperatures for 3 min. 800 μL TMB (0.6 mM) solution was added and reacted for 10 min. The absorbance of samples was recorded at 652 nm using a UV-Vis spectrometer. The effect of pH on the activity of $PdPt_3$-LNT NDs was carried out at 25 ℃ in different pH buffer solution (pH=1-10) with same procedures.

2.5 Catalytic activity retention ability research

The catalytic activity retention ability of $PdPt_3$-LNT NDs under different pH conditions was measured using following steps. 100 μL $PdPt_3$-LNT NDs (C_{pd}=0.078 mM) and 100 μL Hac-NaAc buffer solution (pH=2-10) were mixed and incubated at 25°C for 2 h. 800 μL TMB (0.6 mM) solution and 400 μL Hac-NaAc (pH=4, 0.2 M) buffer solution was added and reacted for 10 min. The absorbance of solution was measured and recorded using a UV-Vis spectrometer. The catalytic activity retention ability of $PdPt_3$-LNT NDs under different NaCl solutions had similar procedures.

2.6 Catalytic kinetics of biomimetic oxidases

100 μL $PdPt_3$-LNT NDs (C_{pd}=0.078 mM) and different doses of Hac-NaAc (pH=4, 0.2 M) buffer solution were transferred in a 2 mL PE tube. The solution was incubated at 40℃ for 3 min. Different volumes of TMB (0.6 mM) solution was further added in the solution. UV-Vis spectrometer was used to record the absorbance at 652 nm.

2.7 Catalytic mechanism of biomimetic oxidases

The existence of hydroxyl radical, superoxide anion and singlet oxygen in the system was measured as follows. All the control experiments were also carried out.

TA was used to detect hydroxyl radicals in $PdPt_3$-LNT NDs and TMB system. 100 μL $PdPt_3$-LNT NDs and 300 μL Hac-NaAc (pH=4, 0.2 M) buffer solution were mixed and incubated at 40°C for 3 min. 800 μL TMB (0.6 mM), 200 μL TA (1 mM) were added and reacted for 10 min. The absorbance at 652 nm was measured. BQ was used to replace TA to detect superoxide anion in $PdPt_3$-LNT NDs and TMB system. The mixed solution of $PdPt_3$-LNT NDs and methylene blue (MB) was used to detect hydroxyl radicals. 100 μL $PdPt_3$-LNT NDs, 500 μL MB (0.01 mM) and 800 μL Hac-NaAc (pH=4, 0.2 M) buffer solution were incubated at 25°C for 3 min. The control experiments were also carried out. The solution of $PdPt_3$-LNT NDs+TMB was added by NaN_3 to detect singlet oxygen**.** 30 μL $PdPt_3$-LNT NDs and 500 μL TMB (0.6 mM) were incubated at 40°C for 3 min, respectively. They were mixed and observed using a UV-Vis spectrometer after the addition of NaN_3 (1 mM) for 6 min.

2.8 Detection of L-cysteine using $PdPt_3$-LNT NDs

Based on the oxidase-like activity of $PdPt_3$-LNT NDs, we established a standard curve for colorimetric detection of L-cysteine. 100 μL $PdPt_3$-LNT NDs (C_{pd}=0.078 mM) and 400 μL Hac-NaAc (pH=4, 0.2 M) buffer solution were incubated at 40°C for 3 min, then 800 μL TMB solution (0.6 mM) and 100 μL L-cysteine solution (0-1000 μM) were added and reacted for 10 min. The data of UV-Vis were recorded. 100 μL milk sample and 100 μL L-cysteine solutions (40, 100, 150 μM) were detected using established method. 10 mM different interfering substances (100 μL) such as glucose, leucine, tyrosine, alanine, phenylalanine, Na^+, K^+ were detected using established method.

3. Results and discussion

3.1 Characterization

The lyophilized LNT was dissolved in deionized water. The weight average molecular weight of LNT was 3.65×10^5 Da based on GPC curve in **Figure S1**. LNT solution was incubated with noble metal precursors at 50 ℃ for 6 h. Some noble metal seeds generated and the addition of ascorbic acid at 60 ℃ for 12 h resulted in the preparation of LNT stabilized metal nanoparticles: Pt-LNT NPs, Pd-LNT NPs, PdPt-LNT NPs, $PdPt_3$-LNT NDs and Pd_3Pt-LNT NPs. **Figure 1 (a)** is the synthesis scheme of $PdPt_3$-LNT NDs. The UV-Vis spectra were shown in **Figure 1 (b)**, K_2PtCl_4 had two peaks in 320 nm and 381 nm. Both characteristic peaks disappeared after treating with LNT and ascorbic acid, which indicated the successful preparation of nanomaterials. Among them, $PdPt_3$-LNT NDs possessed the highest absorbance, implying they may have special morphology [36]. **Figure 1 (c)** is the images of LNT, Na_2PdCl_4, K_2PtCl_4, Pt-LNT NPs, Pd-LNT NPs, PdPt-LNT NPs, $PdPt_3$-LNT NDs, Pd_3Pt-LNT NPs

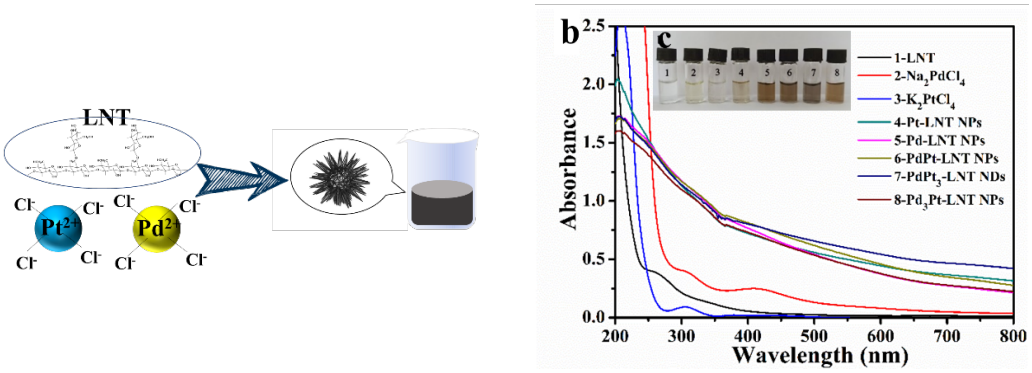

Figure 1 (a) Synthesis scheme of $PdPt_3$-LNT NDs, (b) UV-Vis spectra of samples, (c) images of (1) LNT, (2) Na_2PdCl_4, (3) K_2PtCl_4, (4) Pt-LNT NPs, (5) Pd-LNT NPs, (6) PdPt-LNT NPs, (7) $PdPt_3$-LNT NDs, (8) Pd_3Pt-LNT NPs

The morphology and distribution of the prepared nanomaterials were characterized by TEM. **Figure 2(a)** shows that the morphology of $PdPt_3$-LNT NDs was dendritic nanoparticles and uniformly dispersed. Their particle size was 10.76±1.82 nm in **Figure 2(b)**. This dendritic morphology should be caused by that LNT first reduced some Pd^{2+} to Pd seeds, and then Pt^{2+} preferentially adsorbed on the surface of Pd seeds. Ascorbic acid was added to reduce Pd^{2+} and Pt^{2+} to form PdPt nanoclusters, which were absorbed on the surface of Pd seeds to form $PdPt_3$-LNT NDs in the end. In order to display the

superiority of the biological template LNT, the same amount of deionized water was used to replace LNT to prepare $PdPt_3$ NPs. It can be seen from **Figure 2(c)** that most of $PdPt_3$ NPs aggregated and had a larger size about 20 nm. The reason should be the lack of biological macromolecules LNT. As for $PdPt_3$-LNT NDs, LNT attached and stabilized the metal nanoparticles with dendritic morphology, which may be due to steric structure of LNT. As shown in **Figure 2 (d-g)**, Pt-LNT NPs, Pd-LNT NPs, PdPt-LNT NPs, and Pd_3Pt-LNT NPs were relatively dispersed, which indicated that the biological macromolecule LNT had the function of dispersing nanoparticles well.

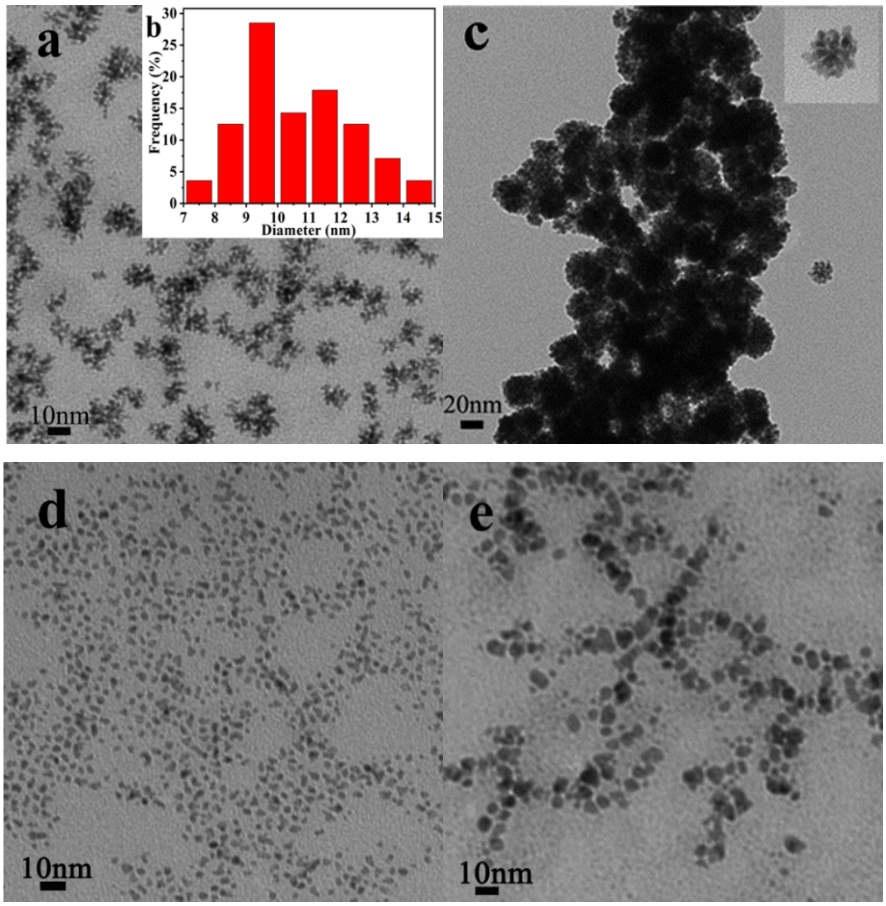

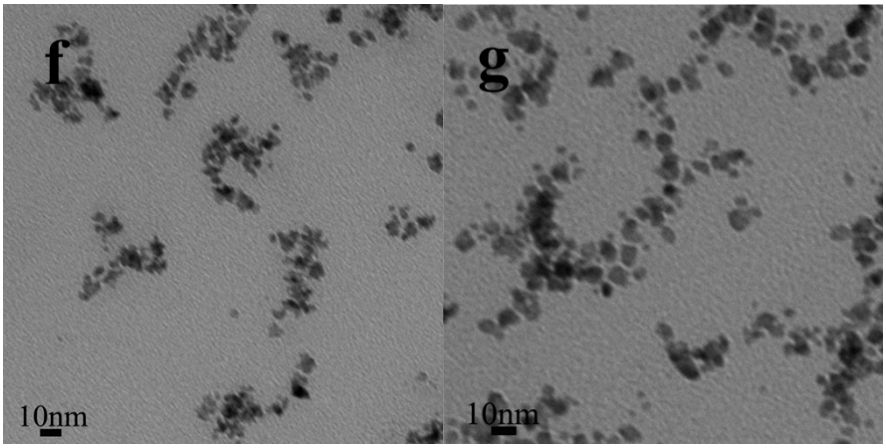

Figure 2 (a) TEM image of $PdPt_3$-LNT NDs, (b) corresponding size statistics, TEM image of (c) $PdPt_3$ NPs, (d) Pt-LNT NPs, (e) Pd-LNT NPs, (f) PdPt-LNT NPs and (g) Pd_3Pt-LNT NPs

FTIR spectra of $PdPt_3$-LNT NDs from 500 cm^{-1} to 4000 cm^{-1} are shown in **Figure 3(a)**. There were obvious peaks at 3383, 2924, 1641, 1371, 1041 and 577 cm^{-1}. Among the peaks, 3383 cm^{-1} was attributed to the stretching vibration of the O-H bond. 2924 cm^{-1} was due to the stretching of the C-H bond. The 1641 cm^{-1} was due to the stretching vibration of the carbonyl group C=O. The 1041 cm^{-1} was due to the stretching vibration of the glycosidic bond. The position at 577 cm^{-1} was attributed to the β-pyranose on the sugar ring. As shown in **Figure 3(b)**, there were four diffraction peaks 39.6°, 46.6°, 67.8°, 81.0° in XRD image of $PdPt_3$-LNT NDs. These four diffraction peaks corresponded to the (111), (200), (220), (311) crystal planes of $PdPt_3$-LNT NDs. The location of diffraction peaks were right in the middle of the diffraction peaks of Pt and Pd [37], which proved the successfully preparation of $PdPt_3$-LNT NDs.

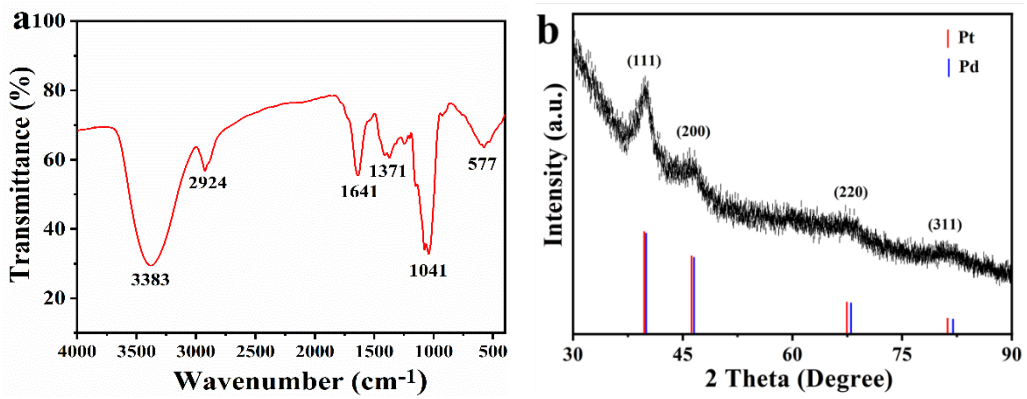

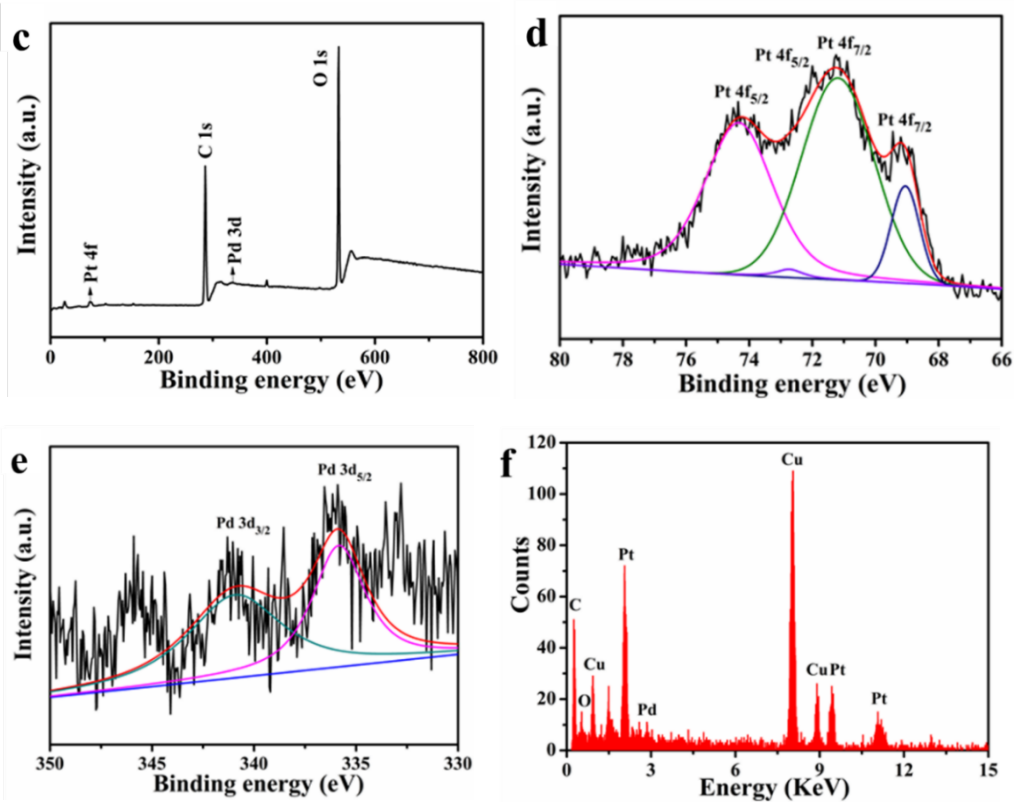

Figure 3 (a) FTIR spectra of $PdPt_3$-LNT NDs, (b)XRD image of $PdPt_3$-LNT NDs, (c)XPS spectrum of $PdPt_3$-LNT NDs, (d) high resolution XPS spectrum of Pt 4f, (e) high resolution XPS spectrum of Pd 3d, (f) EDS image of $PdPt_3$-LNT NDs

XPS was used to research the element composition and valence of $PdPt_3$-LNT NDs. **Figure 3(c)** displays that there were C, O, Pd, Pt elements. C and O elements came from the biological template LNT, Pd and Pt elements came from Na_2PdCl_4 and K_2PtCl_4, respectively. The binding energies of C 1s, O 1s, Pd 3d and Pt 4f were 284.8, 533.08, 335.08 and 73.08 eV, respectively. In **Figure 3(d)**, the corresponding binding energies of Pt 4f $_{5/2}$, Pt 4f $_{5/2}$, Pt 4f $_{7/2}$ and Pt 4f $_{7/2}$ were 74.33, 72.75, 71.19 and 69.05 eV, respectively. **Figure 3(e)** shows two obvious peaks representing Pd 3d $_{3/2}$ and Pd 3d $_{5/2}$, and the corresponding binding energies were 340.93 eV and 335.85 eV, respectively. This result was very similar to the characterization of one-dimensional Pd-Pt bimetallic nanomaterials prepared by Jin et al. Thus, ascorbic acid successfully reduced Pd^{2+} and Pt^{2+} to form zero-valent Pd and Pt in the reaction system to prepare $PdPt_3$-LNT NDs. In order to determine the composition and proportion of each element in $PdPt_3$-LNT NDs, the result of EDS characterization was shown in **Figure 3(f)**. C, O, Cu, Pt, Pd

elements appear, among which C and O were derived from LNT, Cu came from copper mesh, Pd and Pt came from the reduced Na_2PdCl_4 and K_2PtCl_4, and their final atomic percentage of Pd to Pt was 2.07:7.22, which was close to the theoretical ratio of 1:3. In short, these results suggested the successful preparation of $PdPt_3$-LNT NDs.

3.2 Stability in solution

The stability of nanoparticles in water solution is commonly evaluated by the change of hydrodynamic size[38]. In order to explore the stability of $PdPt_3$-LNT NDs under different pH buffer solutions, the hydrodynamic size was characterized by the DLS method. As shown in **Figure 4(a)**, the hydrodynamic size of $PdPt_3$-LNT NDs was about from 22 to 29 nm under different pH buffer solution, which meant $PdPt_3$-LNT NDs had good stability under different pH buffer solutions. **Figure 4(b)** shows that the zeta potential of $PdPt_3$-LNT NDs is between -1.4 mV and -4.9 mV in different buffer solutions, which is smaller than 20 mV. The negative charge on the surface of $PdPt_3$-LNT NDs was derived from the template LNT with negative charge (-4.2 mV). Therefore, the effective stabilization of $PdPt_3$-LNT NDs was due to the fact that the spatial structure of LNT had hindering effect on $PdPt_3$ NDs and the repulsive force between them. The good stability of $PdPt_3$-LNT NDs was good to maintain high catalytic activity in solution.

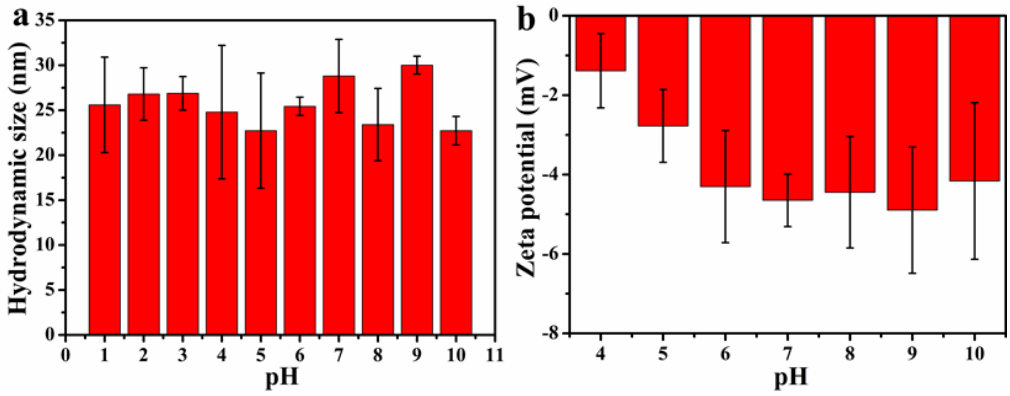

Figure 4 (a) Hydrodynamic size of $PdPt_3$-LNT NDs under different pH buffer solutions and (b) corresponding zeta potential

3.3 Oxidase-like property

In order to evaluate the biomimetic enzyme properties of $PdPt_3$-LNT NDs, we carried

out 5 groups experiments: (1) TMB + Pt-LNT NPs; (2) TMB + Pd-LNT NPs; (3) TMB + PdPt-LNT NPs; (4) TMB + $PdPt_3$-LNT NDs; (5) TMB + Pd_3Pt-LNT NPs. Among them, (4) TMB + $PdPt_3$-LNT NDs show the highest absorbance in these groups in **Figure 5(a)**. **Figure 5(b)** shows that the color of the sample TMB + $PdPt_3$-LNT NDs changed from transparent to blue, which was due to the direct catalytic oxidation of TMB to form oxTMB. Thus, $PdPt_3$-LNT NDs oxidized colorless TMB to a blue oxTMB without hydrogen peroxide, demonstrating their oxidase-like property. $PdPt_3$-LNT NDs had the highest catalytic ability in samples. It may be caused by the fact that $PdPt_3$-LNT NDs had dendritic morphology, good stability, and Pt, Pd in this bimetallic structure had synergistic effect. Synergistic effect exists in palladium and platinum alloys, which improves high catalytic activity of alloys [39,40]. Jin et al report PdPt bimetallic alloy nanowires with Pd:Pt ratio of 1:3 exhibit excellent the most efficient oxidase-like activity. A simple colorimetric assay is developed to detect the acid phosphatase and ascorbic acid based on oxidase-like activity of nanowires [39]. Lai et al prepare polydopamine-mediated magnetic bimetallic nanozyme (Fe_3O_4@PDA@Pd/Pt) with peroxidase-like activity, which is used in immunochromatographic assay. Fe_3O_4@PDA@Pd/Pt has the highest catalytic activity when the ratio of Pt:Pt is 7:3 [40]. It is speculated that the dissolved oxygen in the solution acted as an oxidant, and this reaction was catalyzed by $PdPt_3$-LNT NDs.

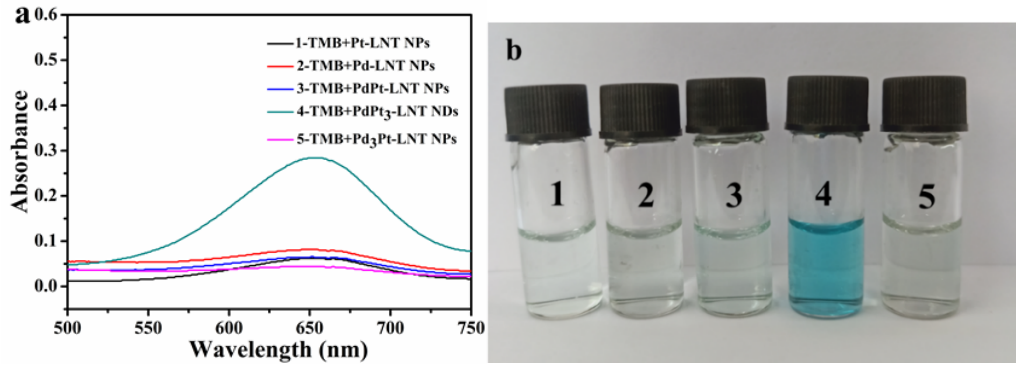

Figure 5 (a) The catalytic activity of Pt-LNT NPs, Pd-LNT NPs, PdPt-LNT NPs, $PdPt_3$-LNT NDs, Pd_3Pt-LNT NPs and (b) corresponding photos

3.4 Optimal temperature and pH

The catalytic activity of nanozymes is affected by environmental factors such as

pH and temperature. Therefore, in order to obtain the optimal reaction temperature and pH value of the solution, we set a series of reaction solution pH (1-10) and reaction temperature (20-70°C). As shown in **Figure 6(a)**, $PdPt_3$-LNT NDs show high relative activity in a weakly acidic environment. When the alkalinity of the reaction solution gradually increased, $PdPt_3$-LNT NDs lost most of their activity. When the pH of the solution was 4, the relative activity of $PdPt_3$-LNT NDs was the highest. It can be seen from **Figure 6(b)** that $PdPt_3$-LNT NDs reached the highest relative activity when the temperature was 40°C. Therefore, the subsequent catalytic reaction proceeded under the conditions of pH 4 and temperature 40°C. In addition, the catalytic activity of nanozymes is closely related with the stability and chemical molecules [41,42] T. Self ea al find that phosphate anions significantly alter the characteristics of CeO_2 nanoparticles [41]. The surface ligands play an important role in the redox properties of CeO_2 nanoparticles [42].

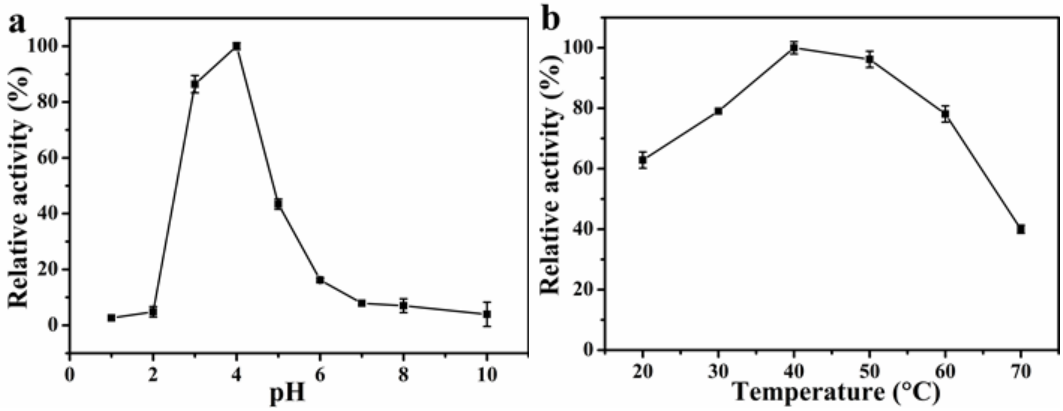

Figure 6 Effect of (a) pH and (b) temperature on the catalytic activity of $PdPt_3$-LNT NDs

3.5 Catalytic activity retention ability

The catalytic activity retention ability of nanoparticles was defined as the remaining catalytic ability of nanoparticles after treating different conditions comparison with original catalytic ability of nanoparticles. The storage of $PdPt_3$-LNT NDs in different environments may have influence on the catalytic activity retention ability of $PdPt_3$-LNT NDs. Therefore, $PdPt_3$-LNT NDs were incubated with buffer solutions of different pH or NaCl solutions of different concentrations for 2 h, and the

catalytic activity retention ability of the biomimetic oxidase of $PdPt_3$-LNT NDs was evaluated. As shown in **Figure 7(a)**, the relative activity of $PdPt_3$-LNT NDs was bigger than 87.19% in the pH range of 2-10. In addition, $PdPt_3$-LNT NDs also maintained excellent catalytic activity (over 90.84%) in 2 M NaCl solution as shown in **Figure 7(b)**. In short, these results proved that $PdPt_3$-LNT NDs had good catalytic activity retention ability in different environments.

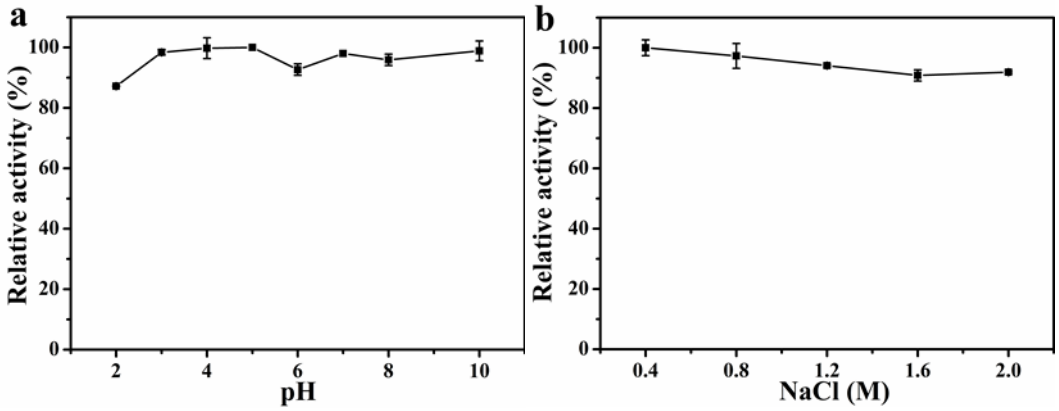

Figure 7 The relative activity of $PdPt_3$-LNT NDs in (a) different pH and (b) different NaCl solution

In order to figure out the catalytic process of $PdPt_3$-LNT NDs, the catalytic kinetics of the reaction was measured under optimal reaction conditions. The kinetic curve was established by changing TMB concentration, and then the typical Lineweaver-Burk double reciprocal plot was used to determine the catalytic kinetic parameters K_m and V_{max} of the $PdPt_3$-LNT NDs. As displayed in **Figure 8(a)**, within the range of substrate TMB concentration (0.129-0.429 mM), the initial reaction rate v increased with increasing TMB concentration. Then the double reciprocal plot method was used to obtain the standard curve of catalytic kinetics as shown in **Figure 8(b)**. The standard equation was y=0.0912x+0.3466 (R^2=0.985), and the kinetic parameters K_m and V_{max} were 0.263 mM and 2.88×10^{-8} $M\cdot s^{-1}$ in Table S1, respectively. K_{mTMB} (0.263 mM) of $PdPt_3$-LNT NDs was smaller than many nanozymes such as BiW_9Cu_3 (0.29 mM), Cu-Ag/rGO (0.634 mM), lysozyme-PtNPs (0.63 mM), which indicated that $PdPt_3$-LNT NDs prepared by us had bigger affinity towards the substrate TMB, which was conducive to efficient catalytic reactions of TMB.

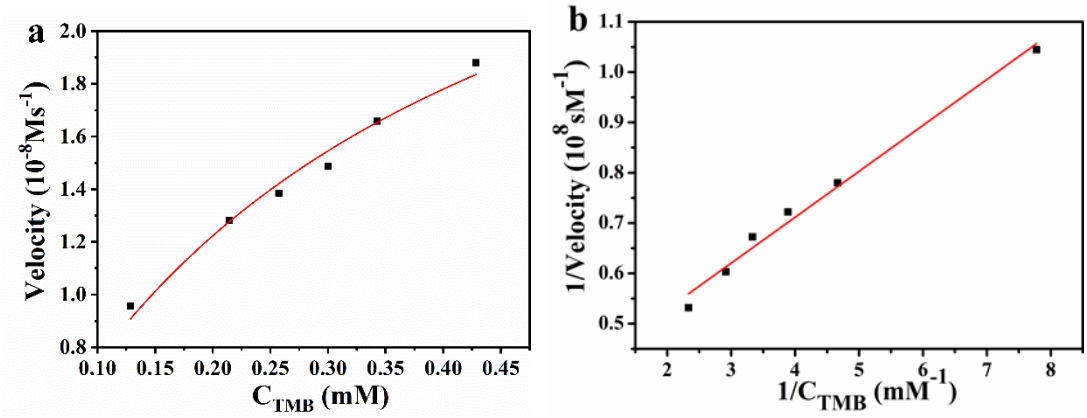

Figure 8 (a) The catalytic kinetics curve of $PdPt_3$-LNT NDs at different concentrations of TMB, (b) double reciprocal curve graph of (a)

3.6 Catalytic mechanism

In order to figure out the catalytic mechanism, TA was used as a quencher of hydroxyl radicals (·OH). TA were incubated with $PdPt_3$-LNT NDs+TMB, and UV-Vis spectrometer recorded the absorbance at 652 nm. **Figure 9(a)** shows that the absorbance of $PdPt_3$-LNT NDs+TMB group and $PdPt_3$-LNT NDs+TMB+TA group was 0.350 and 0.346, respectively. Compared with the blank group, TA had little effect on the absorbance of $PdPt_3$-LNT NDs+TMB group. In addition, BQ were used as a quencher of superoxide anions ($\cdot O_2^-$) [43]. BQ was incubated with $PdPt_3$-LNT NDs+TMB. As displayed in **Figure 9(a)**, the absorbance of $PdPt_3$-LNT NDs+TMB group and $PdPt_3$-LNT NDs+TMB+BQ group was 0.350 and 0.133, respectively. The absorbance of $PdPt_3$-LNT NDs+TMB+BQ group was 38% absorbance of $PdPt_3$-LNT NDs+TMB group. Thus, BQ had obvious inhibition of catalytic oxidation of TMB, which indicated that $PdPt_3$-LNT NDs catalyzed O_2 to produce a lot of $\cdot O_2^-$. This result is consistent with the catalytic mechanism of the $Co_4S_3/Co(OH)_2$ nanotube prepared by Wang et al[44].

After the sample was incubated with methylene blue (MB), the change in absorbance at 664 nm was observed to determine the production of ·OH. It can be seen from **Figure 9(b)** that MB has a maximum absorption peak at 664 nm. When MB was incubated with $PdPt_3$-LNT NDs, there is almost no change in the absorbance at the maximum absorption peak, which indicated that there was no ·OH in the process. **Figure 9(c)** shows that the relative activity of $PdPt_3$-LNT NDs+TMB+ N_2 group was

63.0%, which indicated that O_2 played an important role in the oxidase-like property. Furthermore, the relative activity of $PdPt_3$-LNT NDs+TMB+ NaN_3 group was 31.7%, which suggested the generation of $^1O_2$ due to the fact that NaN_3 captured $^1O_2$ in the catalytic process. To sum up, there was almost no formation of ·OH in this reaction system, $\cdot O_2^-$ and $^1O_2$ were the main reactive oxygen species generated from O_2.

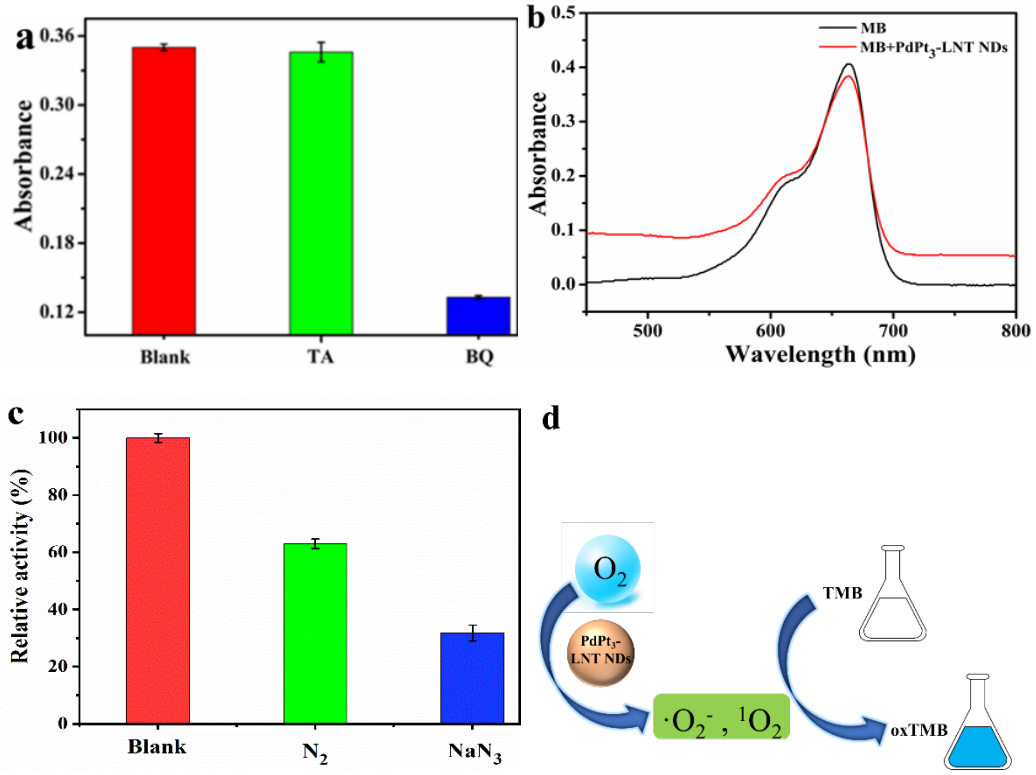

Figure 9 (a) Catalytic mechanism study of $PdPt_3$-LNT NDs using TA and BQ, (b) catalytic mechanism study using MB for detection of ·OH, (c) catalytic mechanism investigation using N_2 and NaN_3, (d) catalytic process of $PdPt_3$-LNT NDs

3.7 L-cysteine detection

L-cysteine is an indispensable amino acid in the human body and plays an important role in a variety of physiological functions. If the content of L-cysteine is abnormal, it will cause various physiological diseases. Therefore, the sensitive detection of L-cysteine has become a research hotspot. The nanozyme activity of $PdPt_3$-LNT NDs was inhibited by the interaction between the metal atoms on the surface of $PdPt_3$-LNT NDs and the -SH in L-cysteine. This made L-cysteine inhibit the oxidation of TMB in the presence of $PdPt_3$-LNT NDs. We have developed a facile and effective

colorimetric method to determine the content of L-cysteine based on this mechanism.

From **Figure 10 (a)**, we found that when L-cysteine was added to the reaction system of $PdPt_3$-LNT NDs and TMB, the color of the solution gradually evolved from light blue to colorless, corresponding to the absorbance at 652 nm reduced significantly, suggesting that the addition of L-cysteine hindered the oxidation of TMB. Because of this phenomenon, we developed a colorimetric method for detecting L-cysteine. In addition, it can be seen from **Figure 10(b)** that when the concentration of L-cysteine is in the range of 0-200 μM, a linear relationship exists between absorbance and concentration. The standard equation is obtained by fitting the curve as y =0.749-0.0034x (R^2=0.9927), the detection limit is 3.099 μM.

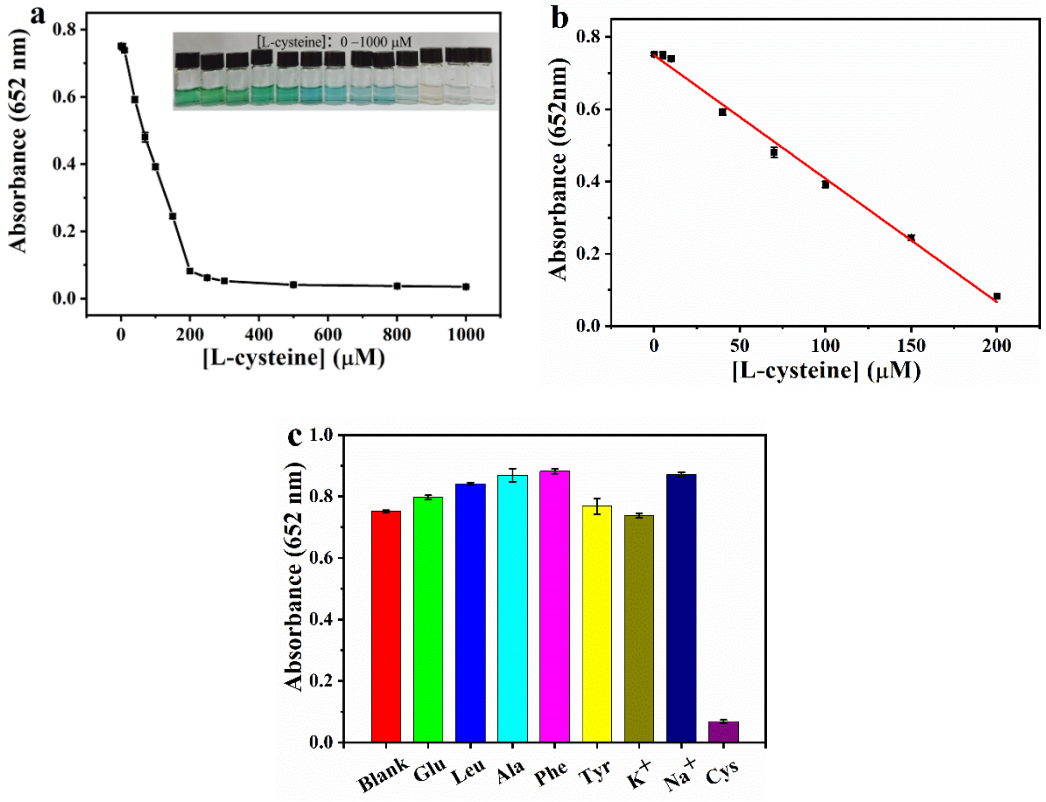

Figure 10 (a) The absorbance changes of reaction solution with L-cysteine concentration (0-1000 μM), (b) standard curve of absorbance with L-cysteine concentration (0-200 μM), (c) the selectivity of L-cysteine detection method on interfering agents

As shown in **Table S2**, the performance of our colorimetric method was compared with other methods. $PdPt_3$-LNT NDs (0-200 μM) have a wider linear range than other

sensors including VS_4 (5-100 μM), POMOF/SWNT nanocomposites (1-80 μM), and Fe^{3+} (0-50 μM). In addition, $PdPt_3$-LNT NDs have a lower detection limit (3.099 μM) than Cu@Au/Pt nanocomposites (4 μM). Therefore, the colorimetric method has wide linear detection range and a sensitive detection limit. There may be interference from other amino acids and ions during detection, selectivity experiment was designed. As shown in **Figure 10(c)**, the absorbance of L-cysteine is much smaller than other interference agents. In addition, the concentration of other interfering agents was 10 mM. Therefore, glucose, amino acids (leucine, alanine, phenylalanine, tyrosine) and ions (K^+, Na^+) did not interfere the L-cysteine detection. Therefore, this method has good anti-interference ability and selectivity, which ensures the accuracy of the detection results. L-cysteine and glutathione are reducing agents, they have different reducing ability [45]. Xiao and coworkers report the presence of glutathione (1 mM) has a certain effect on the detection of L-cysteine [20 μM] [46]. In order to further confirm the reliability of the colorimetric sensor we proposed, L-cysteine in milk sample was also detected. The recovery rate was studied by adding a known amount of standard L-cysteine solution to the milk sample. The results are shown in **Table S3**. The recovery rate of milk samples is 101.40 %-106.54 %, indicating that the developed L-cysteine determination method is feasible and reliable.

4. Conclusion

In summary, bimetallic $PdPt_3$-LNT NDs had good monodispersity, dendritic morphology and good stability, and super oxidase-like property, which was due to the component of LNT. LNT was used to stabilize metal nanoparticles and generate seeds, and ascorbic acid was acted as reducing agent to synthesize $PdPt_3$-LNT NDs (10.76±1.82 nm). $PdPt_3$-LNT NDs had a special dendritic morphology and element ratio (Pd:Pt=2.07:7.22). $PdPt_3$-LNT NDs had good biomimetic oxidase properties, and the catalytic mechanism was that O_2 was catalyzed to $\cdot O_2^-$ and $^1O_2$ by $PdPt_3$-LNT NDs, which oxidized TMB to produce blue oxTMB. More importantly, taking advantage of the catalytic performance of $PdPt_3$-LNT NDs reduced by L-cysteine, a colorimetric method for the detection of L-cysteine was established. The linear range was 0-200 μM,

and the detection limit was 3.099 μM. The measured recovery rate of L-cysteine was 101.40 %-106.54 %. Therefore, bimetallic $PdPt_3$-LNT NDs will have further applications in catalysis and detection.

Acknowledgments

This research was funded by Natural Science Foundation of Hebei Province (B2017203229).

Conflicts of Interest:

The authors declare no conflict of interest.

Corresponding Author

Notes liangbo@ysu.edu.cn, lgwang@ysu.edu.cn

Supplementary data

Figure S1, Table S1, Table S2, and Table S3 are in supplementary data.

Reference:

[1] B.H. Kumar, M.K. Okla, M.A. Abdel-maksoud, W.H. Al-Qahtani, H. AbdElgawad, M.S. Altukhayfi, A.M. Thomas, L.L. Raju, S.S. Khan, Chitosan capped Ag/NiS nanocomposites: A novel colorimetric probe for detection of L-cysteine at nanomolar level and its anti-microbial activity, Int. J. Biol. Macromol. 193 (2021) 2054-2061.

[2] K.M. Fonseca, D.M. RodriguesCosta, V.F. da Silva, J.L. de Carvalho, A.P. Oliveira, F.B.D. Sousa, A.L.F. Lopes, C.D. Martins, L.D. Chaves, L.A.D. Nicolau, G.S. Cerqueira, J.V.R. Medeiros, Anti-inflammatory effect of l-cysteine (a semi-essential amino acid) on 5-FU-induced oral mucositis in hamsters, Amino Acids 53(9) (2021) 1415-1430.

[3] S. Zhang, H. Zhou, N. Kong, Z.Z. Wang, H.M. Fu, Y.H. Zhang, Y. Xiao, W.R. Yang, F.H. Yan, L-cysteine-modified chiral gold nanoparticles promote periodontal tissue regeneration, Bioact. Mater. 6(10) (2021) 3288-3299.

[4] Z.L. Huang, Y.F. Yang, Y.J. Long, H.Z. Zheng, A colorimetric method for cysteine determination based on the peroxidase-like activity of ficin, Anal. Methods.10(23)

(2018) 2676-2680.

[5] N.E.T. Castillo, E.M. Melchor-Martinez, J.S.O. Sierra, N.M. Ramirez-Torres, J.E. Sosa-Hernandez, H.M.N. Iqbal, R. Parra-Saldivar, Enzyme mimics in-focus: Redefining the catalytic attributes of artificial enzymes for renewable energy production, Int. J. Biol. Macromol.179 (2021) 80-89.

[6] Z.S. Han, L. Dong, J. Zhang, T.M. Cui, S.F. Chen, G.L. Ma, X.L. Guo, L.G. Wang, Green synthesis of palladium nanoparticles using lentinan for catalytic activity and biological applications, RSC Adv. 9(65) (2019) 38265-38270.

[7] H. Wei, E.K. Wang, Nanomaterials with enzyme-like characteristics (nanozymes): next-generation artificial enzymes, Chem. Soc. Rev. 42(14) (2013) 6060-6093.

[8] J. Han, J. Yoon, Supramolecular nanozyme-based cancer catalytic therapy, ACS Appl. Energy Mater. 3(11) (2020) 7344-7351.

[9] J.L. Sang, R.L. Wu, P.P. Guo, J. Du, S.M. Xu, J.D. Wang, Affinity-tuned peroxidase-like activity of hydrogel-supported Fe_3O_4 nanozyme through alteration of crosslinking concentration, J. Appl. Polym. Sci. 133(8)(2016) 10 .

[10] X.F. Cai, M.J. Liang, F. Ma, Z.W. Zhang, X.Q. Tang, J. Jiang, C. Guo, S.R. Mohamed, A.A. Goda, D.H. Dawood, L. Yu, P.W. Li, Nanozyme-strip based on MnO_2 nanosheets as a catalytic label for multi-scale detection of aflatoxin B-1 with an ultrabroad working range, Food Chem. 377 (2022) 10.

[11] Z. Li, J.W. Zhang, G. Dai, F.F. Luo, Z.H. Chu, X. Geng, P.G. He, F. Zhang, Q.J. Wang, A ratiometric electrochemical biosensor for glycated albumin detection based on enhanced nanozyme catalysis of cuprous oxide-modified reduced graphene oxide nanocomposites, J Mater Chem B 9(45) (2021) 9324-9332.

[12] C. Liu, M. Zhang, H.Q. Geng, P. Zhang, Z. Zheng, Y.L. Zhou, W.W. He, NIR enhanced peroxidase-like activity of Au@CeO_2 hybrid nanozyme by plasmon-induced hot electrons and photothermal effect for bacteria killing, Appl. Catal. B 295 (2021) 10.

[13] Y. Liang, H.C. Li, L.Y. Fan, R.Y. Li, Y.S. Cui, X.B. Ji, H.Y. Xiao, J. Hu, L.G. Wang, Zwitterionic daptomycin stabilized palladium nanoparticles with enhanced peroxidase-like properties for glucose detection, Colloids Surf. A Physicochem. Eng. Asp. 633

(2022) 8.

[14] X.N. Liu, L.J. Huang, Y.P. Wang, J. Sun, T.L. Yue, W.T. Zhang, J.L. Wang, One-pot bottom-up fabrication of a 2D/2D heterojuncted nanozyme towards optimized peroxidase-like activity for sulfide ions sensing, Sens. Actuators B Chem. 306 (2020) 9.

[15] D.D. Li, Q.Q. Guo, L.M. Ding, W. Zhang, L. Cheng, Y.Q. Wang, Z.B. Xu, H.H. Wang, L.Z. Gao, Bimetallic $CuCo_2S_4$ nanozymes with enhanced peroxidase activity at neutral pH for combating burn infections, Chembiochem 21(18) (2020) 2620-2627.

[16] A. Asati, S. Santra, C. Kaittanis, S. Nath, J.M. Perez, Oxidase-like activity of polymer-coated cerium oxide nanoparticles, Angew. Chem., Int. Ed. 48(13) (2009) 2308-2312.

[17] M. Shah, J. Shah, H. Arya, A. Vyas, A. Vijapura, A. Gajipara, A. Shamal, M. Bakshi, P. Thakore, R. Shah, V. Saxena, D. Varade, S. Singh, Biological oxidase enzyme mimetic Cu-Pt nanoalloys: A multifunctional nanozyme for colorimetric detection of ascorbic acid and identification of mammalian cells, Chemistryselect 4(21) (2019) 6537-6546.

[18] J. Ma, G.G. Feng, Y. Ying, Y. Shao, Y.X. She, L.F. Zheng, A.M. Abd Ei-Aty, J. Wang, Sensitive SERS assay for glyphosate based on the prevention of l-cysteine inhibition of a Au-Pt nanozyme, Analyst 146(3) (2021) 956-963.

[19] L. Jin, Y. Sun, L. Shi, C. Li, Y. Shen, PdPt bimetallic nanowires with efficient oxidase mimic activity for the colorimetric detection of acid phosphatase in acidic media, J Mater Chem B 7(29) (2019) 4561-4567.

[20] Y.C. Shi, L.P. Mei, A.J. Wang, T. Yuan, S.S. Chen, J.J. Feng, l-Glutamic acid assisted eco-friendly one-pot synthesis of sheet-assembled platinum-palladium alloy networks for methanol oxidation and oxygen reduction reactions, J Colloid Interface Sci 504 (2017) 363-370.

[21] H. Dong, Y. Fan, W. Zhang, N. Gu, Y. Zhang, Catalytic mechanisms of nanozymes and their applications in biomedicine, Bioconjug Chem 30(5) (2019) 1273-1296.

[22] N. Cheng, Y. Song, M.M.A. Zeinhom, Y.C. Chang, L. Sheng, H.L. Li, D. Du, L.

Li, M.J. Zhu, Y.B. Luo, W.T. Xu, Y.H. Lin, Nanozyme-mediated dual immunoassay integrated with smartphone for use in simultaneous detection of pathogens, ACS Appl. Mater. Interfaces 9(46) (2017) 40671-40680.

[23] S. Velpula, S.R. Beedu, K. Rupula, Bimetallic nanocomposite (Ag-Au, Ag-Pd, Au-Pd) synthesis using gum kondagogu a natural biopolymer and their catalytic potentials in the degradation of 4-nitrophenol, Int. J. Biol. Macromol 190 (2021) 159-169.

[24] H.Y. Yang, Z.P. Sun, X.G. Qin, H.Y. Wu, H.Z. Zhang, G. Liu, Ultrasmall Au nanoparticles modified 2D metalloporphyrinic metal-organic framework nanosheets with high peroxidase-like activity for colorimetric detection of organophosphorus pesticides, Food Chem. 376 (2022) 7.

[25] J.N. Zheng, L.L. He, F.Y. Chen, A.J. Wang, M.W. Xue, J.J. Feng, A facile general strategy for synthesis of palladium-based bimetallic alloyed nanodendrites with enhanced electrocatalytic performance for methanol and ethylene glycol oxidation, J. Mater. Chem. A 2(32) (2014) 12899-12906.

[26] J. Wu, K. Qin, D. Yuan, J. Tan, L. Qin, X. Zhang, H. Wei, Rational design of Au@Pt multibranched nanostructures as bifunctional nanozymes, ACS Appl. Mater. Interfaces 10(15) (2018) 12954-12959.

[27] W. He, Y. Liu, J. Yuan, J.J. Yin, X. Wu, X. Hu, K. Zhang, J. Liu, C. Chen, Y. Ji, Y. Guo, Au@Pt nanostructures as oxidase and peroxidase mimetics for use in immunoassays, Biomaterials 32(4) (2011) 1139-1147.

[28] Z. Zheng, X. Pan, H. Wang, Z. Wu, M.A. Sullivan, Y. Liu, J. Liu, K. Wang, Y. Zhang, Mechanism of lentinan intestinal absorption: Clathrin-mediated endocytosis and macropinocytosis, J. Agric. Food Chem. 69(26) (2021) 7344-7352.

[29] S.S. Gu, J.Y. Xu, W.T.Z. Teng, X. Huang, M. Hao, X.T. Chen, G. Nie, Z. Cui, X.Q. Liu, Y. Zhang, K.P. Wang, Local delivery of biocompatible lentinan/chitosan composite for prolonged inhibition of postoperative breast cancer recurrence, Int. J. Biol. Macromol 194 (2022) 233-245.

[30] S.P. Wasser, Medicinal mushrooms as a source of antitumor and immunomodulating polysaccharides, Appl Microbiol Biotechnol 60(3) (2002) 258-74.

[31] Yangyang, Zhang, and, Sheng, Li, and, Xiaohua, Wang, and, Lina, Advances in lentinan: Isolation, structure, chain conformation and bioactivities, Food Hydrocoll. (2011) 196-206.

[32] Y. Deng, L.-X. Chen, B.-J. Zhu, J. Zhao, S.-P. Li, A quantitative method for polysaccharides based on endo-enzymatic released specific oligosaccharides: A case of Lentinus edodes, Int. J. Biol. Macromol 205 (2022) 15-22.

[33] L. Dong, R.Y. Li, L.Q. Wang, X.F. Lan, H.T. Sun, Y. Zhao, L.G. Wang, Green synthesis of platinum nanoclusters using lentinan for sensitively colorimetric detection of glucose, Int. J. Biol. Macromol 172 (2021) 289-298.

[34] D. Wu, C. Tang, Y. Liu, Q. Li, W. Wang, S. Zhou, Z. Zhang, F. Cui, Y. Yang, Structural elucidation and immunomodulatory activity of a beta-D-glucan prepared by freeze-thawing from Hericium erinaceus, Carbohydr Polym 222 (2019) 9.

[35] S. Zhou, G. Huang, Extraction, derivatization, and antioxidant activity of Morinda citrifolia polysaccharide,Chem Biol Drug Des (2022) 603-608.

[36] M.N. Nadagouda, R.S. Varma, A Greener Synthesis of Core (Fe, Cu)-Shell (Au, Pt, Pd, and Ag) Nanocrystals Using Aqueous Vitamin C, Cryst. Growth Des. 7(12) (2007) 2582-2587.

[37] X.M. Chen, Z.X. Cai, X. Chen, M. Oyama, Green synthesis of graphene-PtPd alloy nanoparticles with high electrocatalytic performance for ethanol oxidation, J. Mater. Chem. A 2(2) (2014) 315-320.

[38] J.F. He, J. Wang, S.B. Gao, Y.S. Cui, X.B. Ji, X.Y. Zhang, L.G. Wang, Biomineralized synthesis of palladium nanoflowers for photothermal treatment of cancer and wound healing, Int. J. Pharm. 615 (2022) 8.

[39]L. Jin, Y. Sun, L. Shi, C. Li, Y. Shen, PdPt bimetallic nanowires with efficient oxidase mimic activity for the colorimetric detection of acid phosphatase in acidic media, J. Mater. Chem. B 7(29) (2019) 4561-4567.

[40] X. Lai, G. Zhang, L. Zeng, X. Xiao, J. Peng, P. Guo, W. Zhang, W. Lai, Synthesis of PDA-mediated magnetic bimetallic nanozyme and its application in immunochromatographic assay, ACS Appl. Mater. Interfaces 13(1) (2021) 1413-1423.

[41] S. Singh, T. Dosani, A.S. Karakoti, A. Kumar, S. Seal, W.T. Self, A phosphate-dependent shift in redox state of cerium oxide nanoparticles and its effects on catalytic properties, Biomaterials 32(28) (2011) 6745-6753.

[42] V. Patel, M. Singh, E.L.H. Mayes, A. Martinez, V. Shutthanandan, V. Bansal, S. Singh, A.S. Karakoti, Ligand-mediated reversal of the oxidation state dependent ROS scavenging and enzyme mimicking activity of ceria nanoparticles, Chem. Commun. 54(99) (2018) 13973-13976.

[43] X. Lai, Y. Shen, S. Gao, Y. Chen, Y. Cui, D. Ning, X. Ji, Z. Liu, L. Wang, The Mn-modified porphyrin metal-organic framework with enhanced oxidase-like activity for sensitively colorimetric detection of glutathione, Biosens. Bioelectron. 213 (2022) 114446.

[44] J. Wang, Y. Wang, D. Zhang, C. Chen, Intrinsic oxidase-like nanoenzyme $Co_4S_3/Co(OH)_2$ hybrid nanotubes with broad-spectrum antibacterial activity, ACS Appl. Mater. Interfaces 12(26) (2020) 29614-29624.

[45] J. Chen, F.H. Xu, Q. Zhang, S.Y. Li, N-doped MoS_2-nanoflowers as peroxidase-like nanozymes for total antioxidant capacity assay, Anal. Chim. Acta 1180 (2021) 338740.

[46] H. Wu, J. Liu, Z. Chen, P. Lin, W. Ou, Z. Wang, W. Xiao, Y. Chen, D. Cao, Mechanism and application of surface-charged ferrite nanozyme-based biosensor toward colorimetric detection of l-cysteine, Langmuir (2022). https://doi.org/10.1021/acs.langmuir.2c00657